ADVANCED ENERGY MATERIALS
www.advenergymat.de

Stable 24.29%-Efficiency $FA_{0.85}MA_{0.15}PbI_3$ Perovskite Solar Cells Enabled by Methyl Haloacetate-Lead Dimer Complex

Sheng Zhan, Yuwei Duan, Zhike Liu,* Lu Yang, Kun He, Yuhang Che, Wenjing Zhao, Yu Han, Shaomin Yang, Guangtao Zhao, Ningyi Yuan, Jianning Ding, and Shengzhong (Frank) Liu**

Formamidinium methylammonium lead iodide ($FAMAPbI_3$) perovskite has been intensively investigated as a potential photovoltaic material because it has higher phase stability than its pure $FAPbI_3$ perovskite counterpart. However, its power conversion efficiency (PCE) is significantly inferior due to its high density of surface detects and mismatched energy level with electrodes. Herein, a bifunctional passivator, methyl haloacetate (methyl chloroacetate, (MClA), methyl bromoacetate (MBrA)), is designed to reduce defect density, to tune the energy levels and to improve interfacial charge extraction in the $FAMAPbI_3$ perovskite cell by synergistic passivation of both C=O groups and halogen anions. As predicted by modeling undercoordinated Pb^{2+}, the MBrA shows a very strong interaction with Pb^{2+} by forming a dimer complex ($[C_6H_{10}Br_2O_4Pb]^{2+}$), which effectively reduces the defect density of the perovskite and suppresses non-radiative recombination. Meanwhile, the Br^- in MBrA passivates iodine-deficient defects. Consequently, the MBrA-modified device presents an excellent PCE of 24.29%, an open-circuit voltage (V_{oc}) of 1.18 V (V_{oc} loss ≈ 0.38 V), which is one of the highest PCEs among all $FAMAPbI_3$-based perovskite solar cells reported to date. Furthermore, the MBrA-modified devices without any encapsulation exhibit remarkable long-term stability with only 9% of PCE loss after exposure to ambient air for 1440 h.

1. Introduction

Organic–inorganic hybrid perovskites have aroused widespread research attention in the last few years because of their outstanding photoelectric properties.[1–3] So far, the power conversion efficiency (PCE) of hybrid perovskite solar cells (PSCs) has made a remarkable breakthrough from 3.8% in 2009 to a certified value over 25.5% in 2021.[4–6] The remarkable high PCE of hybrid PSCs relies on the unique advantages of perovskite materials (high light-absorption coefficient,[7] broad light-absorption range,[8] fast charge-carrier mobility,[9] long diffusion length,[10] tunable bandgap,[11] small exciton binding energy,[12] etc.) and effective structural and surface modifications (compositional engineering, interfacial passivation, additive engineering, etc.).[13–16] Perovskites based on $FA_xMA_{1-x}PbI_3$ (FA, formamidinium; MA, methylammonium) have been widely applied in hybrid PSCs due to their lower bandgap and higher solar light-harvesting efficiency in contrast to $MAPbI_3$.[17–21] Compared with $FAPbI_3$, partial substitution of FA (ionic radius = 2.79 Å) with MA (ionic radius = 2.17 Å) could improve the stability of hybrid PSCs due to the reduced tolerance factor to the appropriate range (0.8–1).[22,23] However, the low-boiling-point MA cations easily escape from the perovskite lattice during the device fabrication process, and the large FA cations are impeded from embedding into the MA vacancies due to their weak interaction with the established lattice, both of which lead to many defects (MA/FA vacancies, undercoordinated Pb^{2+}, and Pb_I antisites) at the surface and interface of the perovskite.[24–26] Those defects always act as non-radiative recombination

S. Zhan, Y. Duan, Z. Liu, L. Yang, K. He, Y. Che, W. Zhao, Y. Han, S. Yang, G. Zhao, S. (F.) Liu
Key Laboratory of Applied Surface and Colloid Chemistry
Ministry of Education
Shaanxi Key Laboratory for Advanced Energy Devices
Shaanxi Engineering Lab for Advanced Energy Technology
School of Materials Science and Engineering
Shaanxi Normal University
Xi'an 710119, P. R. China
E-mail: yuwwei-duan@snnu.edu.cn; zhike2015@snnu.edu.cn; liusz@snnu.edu.cn

The ORCID identification number(s) for the author(s) of this article can be found under https://doi.org/10.1002/aenm.202200867.

N. Yuan, J. Ding
School of Materials Science and Engineering Jiangsu Collaborative Innovation Center of Photovoltaic Science and Engineering Jiangsu Province Cultivation Base for State Key Laboratory of Photovoltaic Science and Technology
Changzhou University
Changzhou 213164, P. R. China

S. (F.) Liu
iChEM
Dalian Institute of Chemical Physics
University of Chinese Academy of Sciences
Dalian National Laboratory for Clean Energy
Chinese Academy of Sciences
Dalian 116023, P. R. China

DOI: 10.1002/aenm.202200867

centers, which are detrimental to charge-carrier transfer and collection, and they further retard the improvement of PCE as well as generate some uncertainties for large-scale fabrication.[27,28]

Recently, significant efforts have been made to suppress the defects and protect the formamidinium methylammonium lead iodide ($FAMAPbI_3$) films by employing various additives (such as inorganic compounds,[29] ionic liquids,[30] organic ammonium salts,[31] and organic small molecules[32,33]) or device engineering.[34–37] Chen et al. introduced hydrazine chloride as an additive into $FAMAPbI_3$ precursor solution to control the perovskite growth orientation and passivate the iodine defects.[38] Dyson et al. reported an ionic liquid additive 1,3-bis(4-vinylbenzyl)imidazolium chloride [(bvbim)Cl] to create a hydrophobic and protective barrier against moisture by in situ accumulation and polymerization at the grain boundaries (GBs) and providing a PCE of 19.92% for $FAMAPbI_3$ PSCs.[39] Boschloo et al. introduced a small amount of cesium acetate (CsAc) into perovskite precursor, and they found that CsAc can be incorporated into the $FAMAPbI_3$ lattice to reduce its strain and achieved an efficiency of 21.26%.[40] Our group developed a polyfluoro organic compound tri(pentafluorophenyl)boron as a surface passivation agent for $FAMAPbI_3$ PSCs, yielding a PCE of 21.60%.[41] We also reported a multifunctional additive (benzylamine)trifluoroboron (BBF) that could bind with Pb^{2+}, I^-, and FA^+ on the surface and GBs of $FAMAPbI_3$ film, affording synergistic passivation of both cation and anion defects, and delivering a high PCE of 23.24%.[42] Although these additives have indeed improved the quality of perovskite films as well as the performance of hybrid PSCs, the obtained PCEs are still lower than those of state-of-the-art $FAPbI_3$ devices with efficiencies over 25%.[5]

Acetate-based additives with functional C=O groups were reported to retard the growth of perovskite crystal for forming high-quality perovskite film and to passivate halide vacancy (V_H) defects at the surface/interface by coordinating the undercoordinated Pb^{2+} ions.[43–46] However, in the reported calculation and analysis results, it is generally believed that one C=O can only coordinate with one Pb^{2+} ion, and there is little research on the actual coordination mode. Additionally, additives containing halogen atoms (F, Cl, Br) are applied to passivate the surface/interface defects like Pb_I antisite, undercoordinated Pb^{2+}, and V_H, and their effectiveness can be attributed to the electronegativity order of halogen atoms (F > Cl > Br > I).[47–50] However, the synergistic passivation effect of the C=O group and halogen atoms on perovskite was rarely reported.

In this work, we explored a new type of bifunctional passivator, methyl haloacetate (MHA) (methyl chloroacetate, MClA; methyl bromoacetate, MBrA), to passivate the surface defects and tune the energy level of PSCs through the synergistic passivation effect of the C=O group and halogen atoms. It is proved that the existence of the C=O/halogen is important not only to passivate undercoordinated Pb^{2+} and V_I defects of the perovskite film but also to change its band structure to improve interfacial charge extraction in hybrid PSCs. More interestingly, it is first found that two MBrA preferentially combine with one Pb^{2+} forming a dimer complex ($[C_6H_{10}Br_2O_4Pb]^{2+}$), leading to more effective passivation of Pb-related defects compared with MClA, which favors forming a monomer with Pb^{2+}. As a result, an MBrA-modified device exhibits lower defect density and yields a high PCE of 24.29% with high V_{oc} of 1.18 V (V_{oc} loss = 0.38 V), J_{sc} of 24.75 mA cm^{-2}, and FF of 82.92%. To the best of our knowledge, this photovoltaic performance is one of the best for $FAMAPbI_3$-based devices. In addition, the device also exhibits superior stability while being operated at the maximum power point and retains 90% of its initial PCE after 600 s tracking. Furthermore, the MBrA-modified PSC exhibits strong environmental stability, maintaining 91% of its initial PCE after storage under ambient conditions for 60 days.

2. Results and Discussion

An electrostatic potential (ESP) analysis of MHA was conducted to illustrate the effect of halide atom on the electron cloudy density of MHA, as shown in Figure S1, Supporting Information. The electron cloud density (ECD) close to C=O group in MHA is higher than that of halide atom, and the ECD close to C=O in MClA is higher than that in MBrA, suggesting that MClA has stronger ability than MBrA to bind with Pb^{2+} forming a monomer complex through Lewis acid and base. X-ray diffraction (XRD) was utilized to explore the effect of MBrA or MClA modification on the crystallinity of perovskite films.[51] As shown in **Figure 1**a, the diffraction peaks located at 13.9°, 28.0°, 31.5°, and 37.7° are ascribed to (110), (220), (310), and (330) planes, respectively, and the peaks have no significant shift with MClA or MBrA modification, which implies that the MBrA or MClA could not enter into the perovskite crystal lattice but is still retained on the surface of the perovskite film. Meanwhile, the diffraction intensity of the (110) planes is gradually enhanced going from the control to the MClA-modified film and to the MBrA-modified film, suggesting that MBrA could significantly improve the crystallinity of the perovskite film. In addition, a representative diffraction peak of δ-phase perovskite (11.4°) was found in the control film, and it was slightly reduced for the MClA-modified film but almost vanished for the MBrA-modified film. The XRD results indicate that MBrA modification of perovskite film can effectively enhance the crystallinity of the perovskite film and suppress the formation of δ-phase perovskite.

The band gap of the perovskite film was verified via an ultraviolet-visible (UV–Vis) spectrophotometer. As shown in Figure 1b, the perovskite films modified by MClA or MBrA show almost the same absorption edge (located at ≈800 nm, E_g^{opt} = 1.56 eV) and intensity as the control film, confirming that the perovskite crystal structure has not changed after modification. The intensity of the XRD diffraction peak is enhanced, but the absorption intensity remains almost unchanged, so the MClA or MBrA surface modification is helpful to improve the crystallinity of the film.

To study the charge recombination and transport process in the perovskite film and at the perovskite/hole transport layer (HTL) interface, the steady-state photoluminescence (PL) spectra and time-resolved PL (TRPL) decay were analyzed. As shown in Figure 1c, the emission peak was observed at 797 nm for these perovskite films with the excitation wavelength of 510 nm. With MBrA modification, the perovskite film exhibits

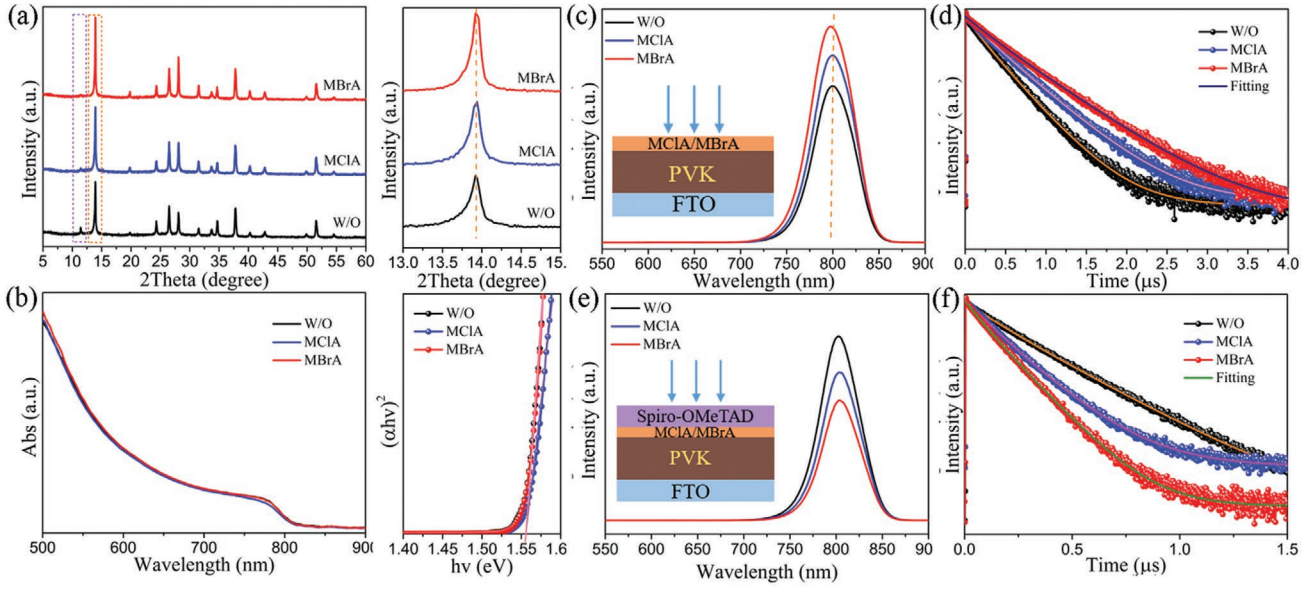

Figure 1. a) XRD patterns, b) UV–Vis absorption spectra, and Tauc plots of perovskite films without and with MHA modification. c) Steady-state PL spectra and d) TRPL curves of glass/perovskite (MHA). e) Steady-state PL spectra and f) TRPL curves of glass/perovskite (MHA)/Spiro-OMeTAD.

the highest PL intensity, indicating the lowest non-radiative recombination, which could be ascribed to the effective passivation effect of MBrA on surface defects of the perovskite film. In addition, the emission peak of MBrA-modified perovskite film shows an obvious blue-shift, indicating that the sub-bandgap states were suppressed.[52] The biexponential equation $F(t) = A_1 \exp(-t/\tau_1) + A_2 \exp(-t/\tau_2) + B$ and corresponding equation $\tau_{ave} = (A_1\tau_1^2 + A_2\tau_2^2)/(A_1\tau_1 + A_2\tau_2)$ were employed to fit the TRPL decay curves (Figure 1d) and deduce the average carrier lifetime (τ_{ave}), where the A_i (i = 1, 2) values correspond to the decay amplitudes, and τ values are the decay time constants. The fitted parameters are summarized in Table S1, Supporting Information. The τ_{ave} was prolonged from 365.12 to 602.81 ns by MBrA modification, indicating a slower recombination rate in the MBrA-modified perovskite film.

PL and TRPL measurements were applied to further clarify the important role of MBrA or MClA modification on the charge-carrier transfer and extraction process at the perovskite/HTL interface.[53] As shown in Figure 1e, the perovskite (MBrA)/Spiro-OMeTAD film shows an obvious fluorescent quenching phenomenon compared with the perovskite/Spiro-OMeTAD and perovskite (MClA)/Spiro-OMeTAD, demonstrating the more efficient charge transfer from perovskite to Spiro-OMeTAD. Figure 1f shows the TRPL results, and the corresponding parameters are summarized in Table S2, Supporting Information. It is known that the fast lifetime (τ_1) is ascribed to the charge-transfer quenching of PL, and the long lifetime (τ_2) originates from the charge-recombination quenching of PL. Both the τ_1 and τ_2 for the perovskite (MBrA)/Spiro-OMeTAD film are faster than those of the perovskite/Spiro-OMeTAD and perovskite (MClA)/Spiro-OMeTAD films, which further confirms that MBrA can accelerate charge transfer from the perovskite to the HTL. Furthermore, the faster charge transfer in the perovskite (MBrA)/Spiro-OMeTAD film was further proved by time-resolved femtosecond transient absorption spectroscopy (fsTA), as shown in Figure S2, Supporting Information.

To understand the effect of MHA modification on the morphology of the perovskite film, scanning electron microscopy (SEM) and atomic force microscopy (AFM) characterizations were performed.[54] Top-view SEM images of perovskite films without and with MHA modification are shown in **Figure 2**a, and the corresponding grain size distributions are summarized in Figure 2b. MClA and MBrA modifications increase the average grain sizes of the perovskite films up to 1020 and 1340 nm, respectively, from 620 nm for the control film. The increase of grain size means a decrease of GBs and surface/interface defects, which is conducive to improving the photovoltaic performance of hybrid PSCs. In addition, the water contact-angle was increased from 59.1° for the control film to 78.5° for the MClA-modified film and 81.4° for the MBrA-modified film. It is well-known that halide atoms, as a strongly hydrophobic group, are widely applied in thin-film solar cells.[55] The increased contact-angle for MBrA-modified film is due to the strong capacity of MBrA to form a complex with Pb^{2+}, causing a great number of Br atoms to be located at the surface of perovskite film. The increased hydrophobicity plays a crucial role in enhancing the stability of PSCs. Cross-sectional SEM images of perovskite films are shown in Figure 2c, where, for the MBrA-modified perovskite film, the grain size increases remarkably, and fewer boundaries are observed, showing perfect single-crystal grains throughout the thickness of the perovskite film, which could enhance the charge-transport efficiency in the vertical direction. AFM images are shown in Figure 2d, where compared with the control and MClA-modified films, the MBrA-modified film shows a smoother surface, which is conducive to better contact between the perovskite and Spiro-OMeTAD.

Fourier-transform infrared (FTIR) spectroscopy was conducted to clarify the interaction between MHA and perovskite. **Figure 3**c shows a typical stretching vibrational peak of C=O from MBrA film located at 1743 cm^{-1}. With the addition of lead iodide (PbI_2) into the MBrA, the C=O peak shifts from 1743 to

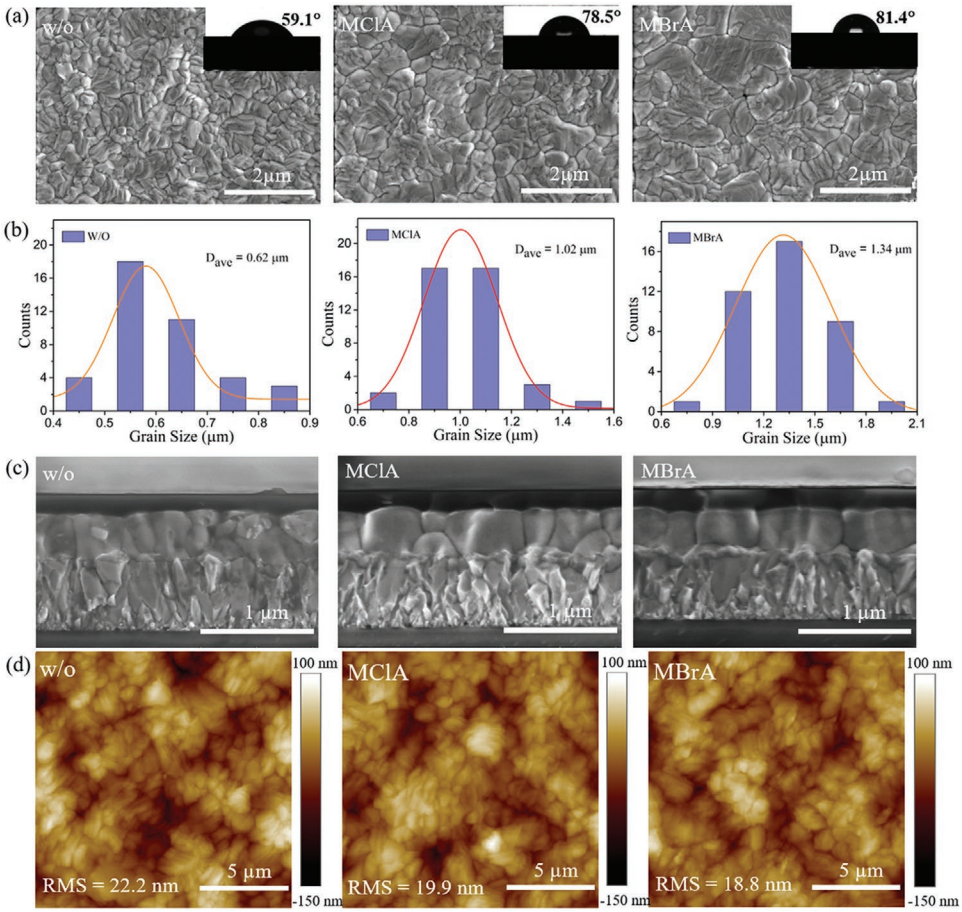

Figure 2. a) Top-view SEM images and water contact angles, b) grain-size distributions, c) cross-sectional SEM images, and d) AFM images of the control, MClA-, and MBrA-modified perovskite films.

1728 cm^{-1} (shifted 15 cm^{-1}), which is due to the electron delocalization in the C=O bond that is aroused by strong interaction between Pb^{2+} and C=O. In Figure 3d, the same movement can be observed from MClA film (1744 cm^{-1}) to MClA + PbI_2 film (1734 cm^{-1}) (shifted 10 cm^{-1}). The smaller movement in MClA + PbI_2 film is probably ascribed to the stronger intermolecular noncovalent interaction of Cl···C=O that weakens the interaction between C=O and Pb^{2+}.[56] The FTIR results indicate that there is a stronger interaction between Pb^{2+} and MBrA. The interaction between perovskite and MHA was further proved by the ^{1}H nuclear magnetic resonance (^{1}H NMR) results. As shown in Figure 3a and Figure S3, Supporting Information, the NMR peak of the $-CH_2-$ bond for MBrA (integration:2) shows an obvious upfield chemical shift of $\Delta\delta \approx 0.02$ ppm (from 4.15 to 4.13 ppm) and becomes very weak with addition of PbI_2, indicating the interaction between C=O and Pb^{2+}. In addition, the integrated area of the weak peak at 4.12 ppm is only 0.5. Interestingly, a new group of strong peaks arises at 3.78 and 3.63 ppm, and the integrated areas of the two new peaks are 4 and 6 (ratio = 2:3), respectively. Therefore, most of the MBrA is converted to other compounds in the MBrA/PbI_2 mixture. In order to confirm the new compound, the solution was analyzed by mass spectrometry (Figure S4, Supporting Information), which shows that a new compound with molecular weight of 511.84 was produced corresponding to the dimer complex $[C_6H_{10}Br_2O_4Pb]^{2+}$. The ratio of the dimer $[C_6H_{10}Br_2O_4Pb]^{2+}$ to the monomer $[C_3H_5BrO_2Pb]^{2+}$ is 8:1, which is determined by the integration of $-CH_2-$ groups. Therefore, in most cases, two MBrA prefer to bind simultaneously with one PbI_2. However, a contrary phenomenon was observed in the mixture of MClA + PbI_2. According to Figure 3b and Figure S5, Supporting Information, the ratio of $[C_6H_{10}Cl_2O_4Pb]^{2+}$ to $[C_3H_5ClO_2Pb]^{2+}$ is only 1:5, which means that only one-fifth of the MClA molecules participate in binding with Pb^{2+} forming the dimer complex, and four-fifths of the MClA molecules prefer to bind with one Pb^{2+} to form the monomer complex. Those results were also confirmed by the above ESP analysis.

As a supplement to the FTIR data, X-ray photoelectron spectroscopy (XPS) measurements were conducted to further unveil the influence of MHA on the perovskite films. As shown in Figure S6, Supporting Information, the $4f_{5/2}$ and $4f_{7/2}$ peaks of Pb^{2+} in the control film are located at 143.13 and 138.24 eV, respectively. With the MClA modification of the perovskite film, both the $4f_{5/2}$ and $4f_{7/2}$ peaks show a slight movement toward lower binding energy, whereas for MBrA-modified film, the $4f_{5/2}$ and $4f_{7/2}$ peaks of Pb^{2+} exhibit an obvious shift to lower binding energy and broaden, indicating there is a strong interaction between MBrA and Pb^{2+}. The XPS results are in

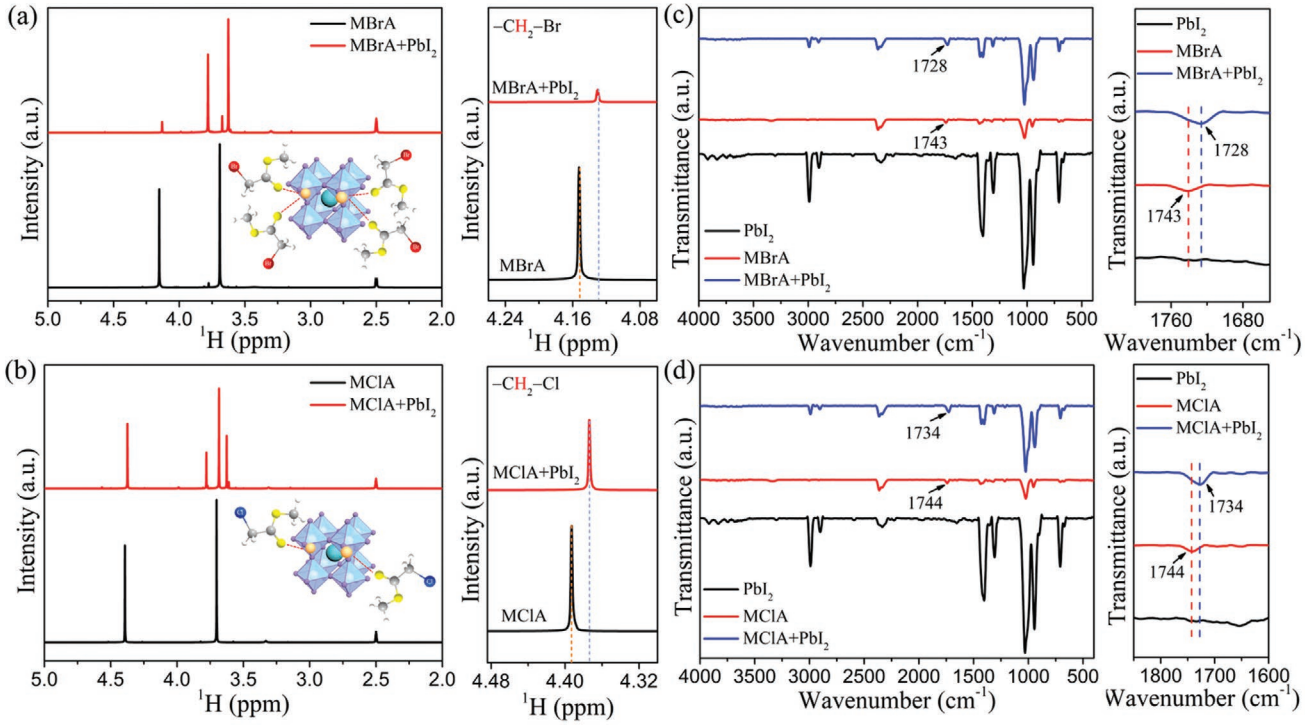

Figure 3. ^{1}H NMR spectra of a) MBrA and b) MClA in DMSO-D_6 solution with and without PbI_2 additive. The FTIR spectra of c) MBrA and d) MClA with and without PbI_2 additive.

agreement with those of the FTIR. In addition, compared with the control and MClA-modified films, the O1s peak originating from both $-C-O-CH_3$ in MBrA and absorbed oxygen in the MBrA-modified film slightly shifts to higher binding energy as a consequence of forming C=O–Pb bonds. There is no Br 3d signal peak for the control film, while there are two obvious signal peaks located at 72.46 and 70.74 eV (corresponding to Br $3d_{3/2}$ and $3d_{5/2}$, respectively) for the MBrA-modified film. However, the Cl 2p peaks could not be detected for either the control or MClA-modified films, which might be due to the Cl atoms easily leaving the surface of the perovskite film during the thermal annealing process.[57]

In order to examine the effect of MHA modification on photovoltaic performance, PSCs with the fluorine-doped tin oxide (FTO)/SnO_2/perovskite(MHA)/Spiro-OMeTAD/Au structure are fabricated, as shown in **Figure 4**a. Ultraviolet photoelectron spectroscopy (UPS) was conducted to explore the impact of MHA modification on the Fermi energy (E_F), conduction band (CB), and valence band (VB) of the perovskite films (Figures S7 and S8, Supporting Information). The detailed parameters of the band structure are summarized in Table S3, Supporting Information. The VB of the control, MClA-, and MBrA-modified perovskite films are extracted as −5.61, −5.58, and −5.47 eV, respectively. Combining the VB with the bandgap (1.56 eV obtained from UV–Vis), the CB are estimated to be −4.05, −4.02, and −3.91 eV for the control, MClA-, and MBrA-modified perovskite films, respectively. The energy level alignments are drawn in Figure 4b. Obviously, the CBs and VBs are gradually shifted up from the control to MClA- and to MBrA-modified perovskite films, which is mainly ascribed to the efficient surface passivation and the formation of interfacial dipoles at the perovskite/HTL interface. The elevated CBs of MBrA-modified perovskite film might facilitate the charge separation and improve the extraction of photogenerated charges from the perovskite to HTL.[58,59] The device performance was optimized by tuning the MClA or MBrA concentrations from 0 to 1%, 2%, 4%, and 8%. According to Figure S9, Supporting Information, and Tables S4 and S5, Supporting Information, the optimal concentration was determined as 2% for both MClA and MBrA. As shown in Figure 4c, the control device exhibited a PCE of 22.26% with V_{oc} of 1.13 V, J_{sc} of 24.55 mA cm^{-2}, and FF of 80.26%. The MClA-modified device shows a higher PCE of 23.56% with V_{oc} of 1.17 V, J_{sc} of 24.60 mA cm^{-2}, and FF of 81.59%. The MBrA-modified device yields a champion PCE of 24.29% with V_{oc} of 1.18 V, J_{sc} of 24.75 mA cm^{-2}, and FF of 82.92%. To the best of our knowledge, this is one of the highest reported PCEs for $FAMAPbI_3$-based PSCs to date.

Compared with the control and MClA-modified devices, the improved performance for the MBrA-modified device mainly arises from the increases of V_{oc} and FF. External quantum efficiency (EQE) measurements were conducted to verify the J_{sc} obtained from the J–V curves. As shown in Figure 4d, the integrated current densities (J_{cal}) obtained from EQE curves are 24.20, 24.49, and 24.51 mA cm^{-2} for the control, MClA-, and MBrA-treated devices, respectively, which agree well with the J_{sc} obtained from the corresponding J–V curves.

The statistical distributions of photovoltaic parameters for 40 devices of each type are shown in Figure S10, Supporting Information. The average PCE is remarkably improved from the control device 21.88% to the MBrA-treated device 24.00%, which further confirms that the perovskite devices modified by MBrA have not only better performance but better reproducibility in contrast to the other devices. The stabilized

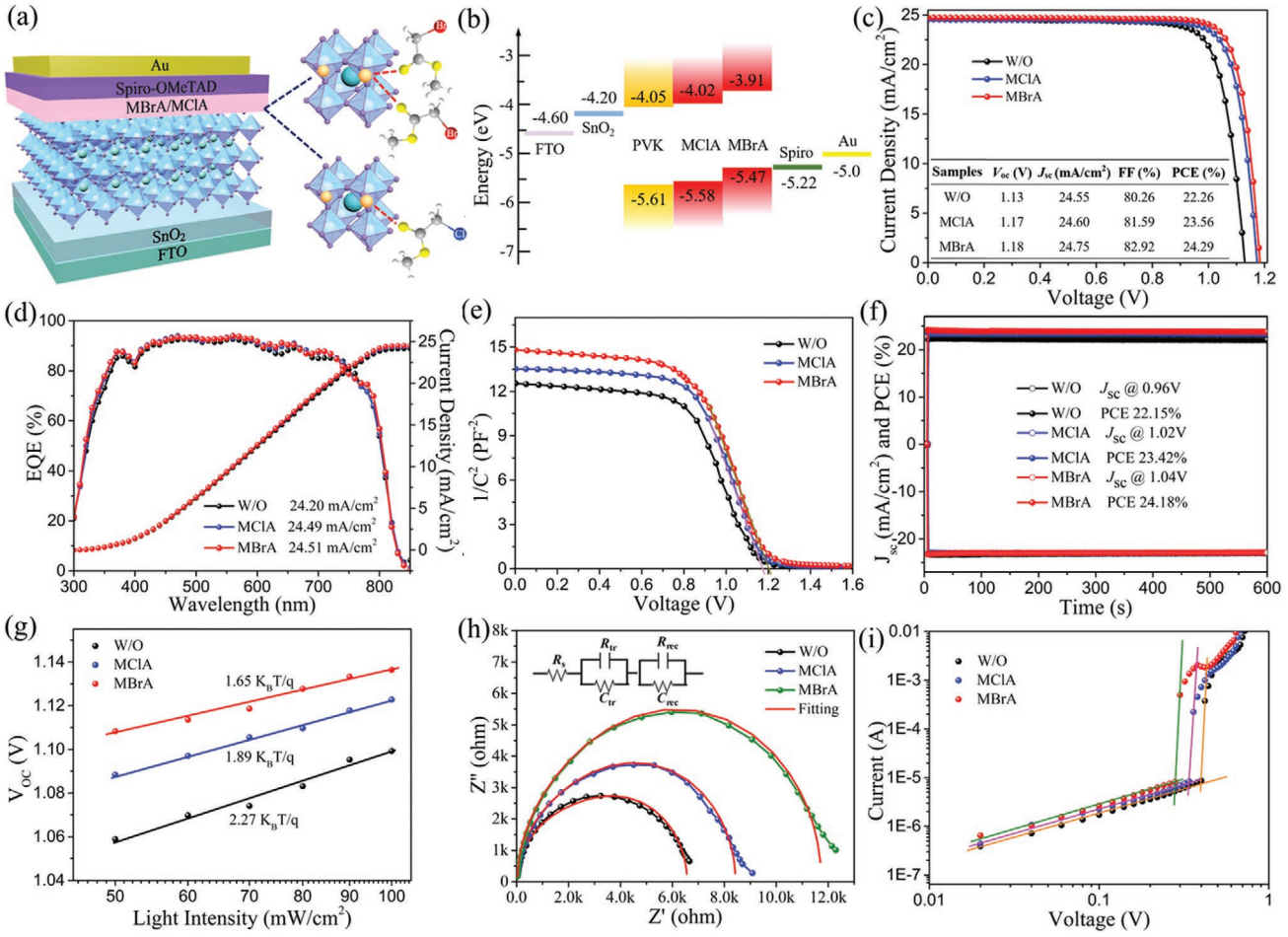

Figure 4. a) The device structure, b) schematic energy level alignment, c) *J–V* curves of champion PSCs, d) external quantum efficiency (EQE) spectra of devices, e) *C–V*, f) maximum power-point tracking of the champion devices, g) V_{oc} dependence on light intensity, h) Nyquist plots, and i) the space-charge-limited current versus voltage for the control, MClA-, and MBrA-modified devices.

maximum-power-point (MPP) output for control, MClA-, and MBrA-modified devices were tested with the devices biased at 0.96, 1.02, and 1.04 V, respectively. As shown in Figure 4f, the stabilized PCE for the MBrA-treated device is estimated to be 24.18% for a testing period of 600 s, which is in accord with the PCE from *J–V* measurements. The increased V_{oc} of the MClA- and MBrA-modified devices can be attributed to the improved built-in potential (V_{bi}) that was caused by the elevated CB of the perovskite film, which was confirmed by Mott–Schottky analysis.[60] As shown in Figure 4e, the V_{bi} of control, MClA-, and MBrA-modified PSCs are 1.14, 1.17, and 1.20 V, respectively. Therefore, the MBrA modification can enhance the CB of the perovskite to increase the V_{bi} of the PSCs leading to higher V_{oc}.

The curve of the relationship between V_{oc} and light intensity was carried out to evaluate the charge carrier recombination mechanism of devices by the slope of curve and further to elucidate the reason for improved FF in Figure 4g. The slope of the curve is associated with the Shockley–Read–Hall (SRH) recombination assisted by trap density in PSCs. The MBrA-modified perovskite film has the smallest slope of 1.65 kT q^{-1} compared with the control and MClA-modified devices, manifesting that the trap-assisted SRH recombination was efficiently suppressed by MBrA modification and resulting in the promoted FF. Electrochemical impedance spectroscopy (EIS) measurement was conducted to investigate the charge-transfer properties.[61] As shown by the Nyquist plots in Figure 4h and the fitting parameters summarized in Table S6, Supporting Information, the MBrA-modified device exhibits the lowest series resistance (R_s) of 29.16 Ω and transfer resistance (R_{tr}) of 1452 Ω and the largest recombination resistance (R_{rec}) of 1.025×10^4 Ω among the three devices, which further illustrates that the MBrA modification is beneficial to suppressing the charge recombination and facilitating efficient charge transfer. It is speculated that the highly efficient charge transfer originates from the reduced surface defect density. For quantitatively evaluating the reduction of surface defect density in the perovskite film, an electron-only device with a structure FTO/TiO_2/perovskite (MHA)/$PC_{61}BM$/Ag was fabricated. The trap-state-density (N_t) was determined via a space-charge limited current method in the dark. The N_t can be calculated from the trap-filled limit voltage (V_{TFL}).[24] As shown in Figure 4i and Table S7, Supporting Information, the V_{TFL} for the control film is 0.40 V, corresponding to N_t of 1.01×10^{16} cm^{-3}. Obviously, the V_{TFL} and N_t simultaneously decline with the MClA or MBrA modification. The N_t of MClA- and MBrA-modified perovskite films are 8.62×10^{15} and

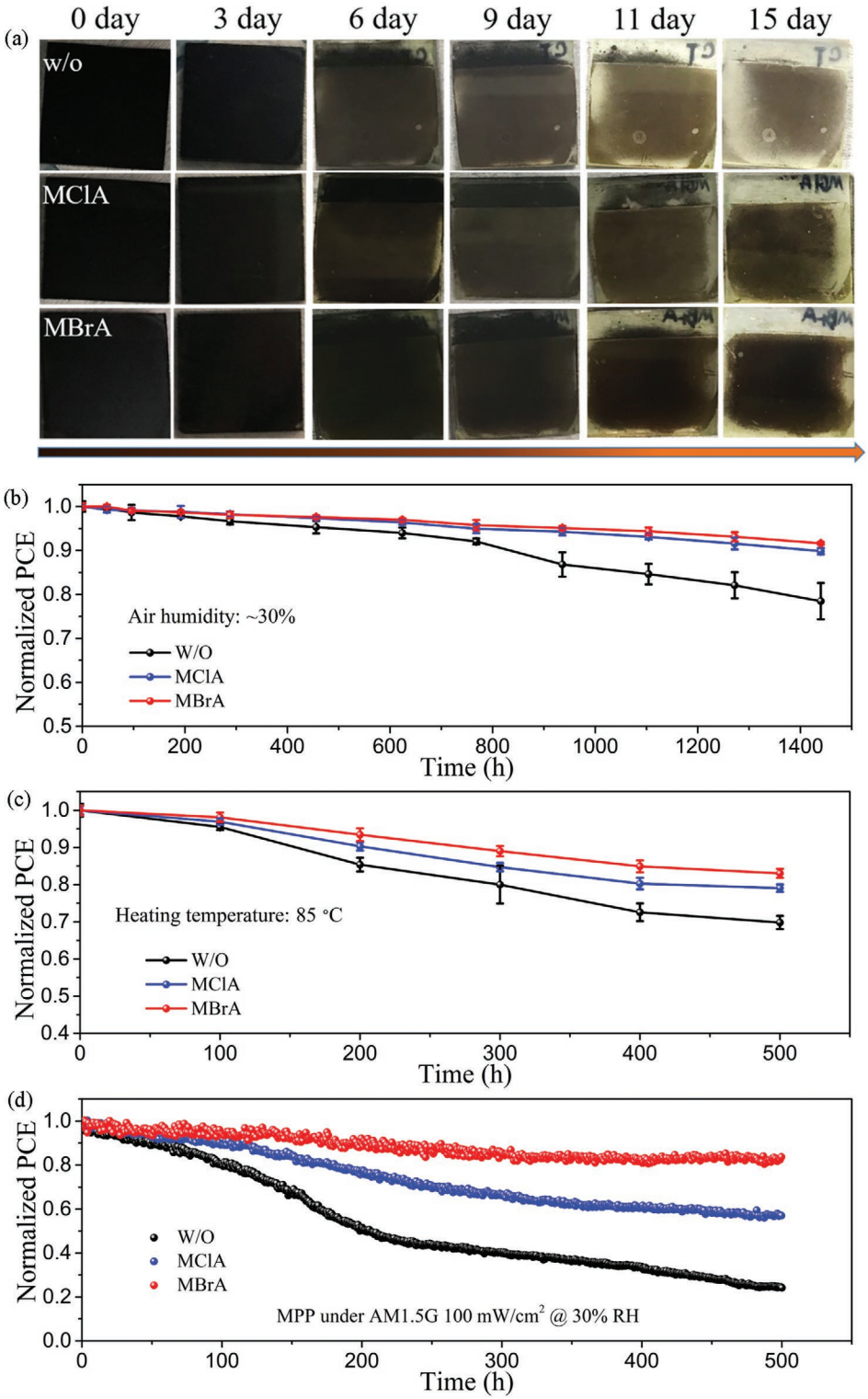

Figure 5. a) Photographs of control, MClA-, and MBrA-modified perovskite films aged in ambient air with a relative humidity of ≈30%. b) The air stability of the control, MClA-, and MBrA-modified PSCs in air for 1440 h. c) The thermal stability (T = 85 °C in N_2 atmosphere) of the control, MClA-, and MBrA-modified PSCs. d) The MPP tracking of encapsulated control, MClA-, and MBrA-modified PSCs.

7.10×10^{15} cm^{-3} with the V_{TFL} of 0.34 and 0.28 V, respectively. The lowest N_t of MBrA-modified perovskite film can be ascribed to the strong interaction between MBrA and Pb^{2+}, which is helpful to passivate the surface defects of the perovskite film.

To investigate the MClA or MBrA modification on the stability of the perovskite film, unencapsulated perovskite films were stored in ambient conditions (humidity ≈ 30%; and temperature = 25 °C) for different durations.[62] As shown in **Figure 5**a,

the MBrA-modified film can maintain its dark black appearance after exposure to air for 15 days, which was far longer than the control film (becomes semi-transparent after 6 days) and MClA-treated film (becomes semi-transparent after 9 days). The long-term environmental stability of the PSCs was also investigated in ambient conditions. As shown in Figure 5b, it is clear that the unencapsulated MBrA-modified and MClA-modified devices maintain 91% and 89%, respectively, of their initial PCEs after storage for 1440 h in air, which is obviously higher than that of the control device (78%). Thermo-stability measurement of unencapsulated devices was carried out under N_2 atmosphere at 85 °C, as shown in Figure 5c. The MBrA-modified devices maintained 83% of their initial PCEs after continuous heating for 500 h, which is higher than the 79% for MClA-modified devices and 69% for the control devices. In order to further investigate the effect of MClA or MBrA modification on the operational stability of PSCs, the encapsulated devices were exposed to continuous one-sun illumination under ambient conditions. As shown in Figure 5d, the MBrA-treated device maintained 82% of its initial PCE after MPP tracking for 500 h, which is obviously higher than 56% for MClA-treated device and 24% for control device.

3. Conclusion

In summary, we adopt two smart molecules (MClA and MBrA), each with both a C=O group and halide anion, to improve the efficiency and stability of $FAMAPbI_3$ PSCs. Compared with control and MClA-modified devices, the MBrA-modified PSCs yield a champion PCE of 24.29% with J_{sc} of 24.75 mA cm^{-2}, V_{oc} of 1.18 V, and FF of 82.92%. On the one hand, the MBrA modification could tune the energy level of the perovskite film to be well-matched with the HTL layer so as to facilitate charge carrier extraction and transfer. On the other hand, compared with MClA, two MBrA molecules prefer to bind with one Pb^{2+} ion on the surface/interface of perovskite film to more efficiently passivate the undercoordinated Pb^{2+} defects and further improve the V_{oc} and FF of the PSCs; at the same time, the Br^- anions efficiently passivate iodine-related defects and prevent moisture permeation into the device by improving the hydrophobicity of the perovskite film. The MBrA-modified PSC maintains 91% of its initial PCE after storage for 1440 h in ambient air conditions. Furthermore, the encapsulated device treated by MBrA maintains 82% of its initial PCE after exposing to continuous one-sun illumination under atmospheric conditions.

4. Experimental Section

Materials: MBrA, MClA, *N*,*N*-dimethylformamide (DMF, 99.8%), cesium iodide (99.999%), chlorobenzene, and dimethylsulfoxide (DMSO, 99.9%) were purchased from Shanghai Aladdin Biochemical Technology Co. Ltd. Tin(IV) oxide (SnO_2), 15% in H_2O colloidal dispersion liquid were purchased from Alfa Aesar. 4-*tert*-butylpyridine (*t*-BP) and bis(trifuoromethylsulfonyl)imide lithium salt (Li-TFSI) were purchased from Sigma-Aldrich. PbI_2, methylammonium iodide (MAI), formamidinium iodide (FAI), and methylammonium chloride were purchased from Xi'an Polymer Light Technology Corp.

Device Fabrication: FTO/glass substrates were successively cleaned by ultra-sonication in a special cleaning concentration (mixed detergent and ultrapure water of 1:100) for 30 min and ultrapure water for 30 min, and the above processes were repeated twice. Then the substrates were dried by nitrogen flow and treated with ultraviolet light for 10 min before deposition of SnO_2. The cleaned substrates were further treated with ultraviolet ozone plasma for 15 min. Next, SnO_2 colloid water precursor was diluted with H_2O by a certain proportion, the diluted precursor was spun on the substrates at 3000 rpm for 40 s, and the obtained SnO_2 substrates were annealed at 200 °C for 30 min and treated with ultraviolet light for 10 min to improve the wettability. The $FA_{0.85}MA_{0.15}PbI_3$ precursor solution was prepared by dissolving FAI, MAI, and PbI_2 (molar ratio = 0.85:0.15:1) in DMF and DMSO (4:1 v/v). The resulting solution was filtered through a 0.45 µm syringe filter before use. The perovskite precursor solution was spun at 1000 rpm for 10 s, followed by 4000 rpm for 40 s while dripping diethyl ether onto the substrate 30 s before the end of the program. Afterward, the film was annealed at 150 °C for 10 min to obtain the perovskite layer. The MBrA or MClA was dissolved in chlorobenzene at different volume ratios (1%, 2%, 4%, 8% v/v) and stirred for 6 h. For surface treatment, 60 µL MBrA or MClA solution was deposited onto perovskite film at 5000 rpm for 30 s and then annealed at 80 °C for 5 min. After cooling to room temperature, 40 µL of Spiro-OMeTAD solution composed of 90 mg Spiro-OMeTAD, 36 µL t-BP, and 22 µL Li-TFSI (520 mg mL^{-1} in acetonitrile) in 1 mL of chlorobenzene was spin-coated at 5000 rpm for 30 s to prepare the HTL. Finally, 80 nm of Au was thermally deposited as the electrode by vacuum evaporation. The active area of each device was 0.09 cm^2. The mask with an area of 0.07 cm^2 was used for *J*–*V* and I-T testing.

Characterization: FTIR spectra were obtained with a PE-Frontier, and DMSO was used as the solvent to dissolve PbI_2, MBrA or MClA, and PbI_2 + MBrA or MClA. ^{1}H-NMR spectra were acquired by a JNM-ECZ400S/L1 with a frequency of 400 MHz, using samples formed by dissolving the same molar quantity of MHA, and MHA + PbI_2 into 0.5 mL DMSO-D_6, respectively. The solution of PbI_2 and MBrA or MClA dissolved in 50 µL DMSO and 200 µL CH_2Cl_2 was used for mass spectroscopy, which was performed using a MALDI-TOF mass spectrometry. XPS was performed on a photoelectron spectrometer (ESCALAB 250Xi, Thermo Fisher Scientific). The band structures of the perovskite films were analyzed via UPS (ESCALAB 250Xi, Thermo Fisher). SEM images of perovskite films were obtained by field-emission SEM (HITACHI, SU-8020). Water contact angles of perovskite films were measured through a DataPhysics OCA 20. The AFM images were acquired using a Veeco NanoScope IV with a silicon cantilever. XRD patterns for perovskite films were obtained from a D/MAX 2400 diffractometer with Cu Kα radiation (Rigaku). Absorption spectra of perovskite films were acquired by a UV/vis NIR spectrophotometer (Ocean Optics Instrument). PL (excitation at 532 nm) spectra were measured using an Edinburgh Instruments Ltd. FLS980 spectrometer under 510 nm-wavelength excitation. TRPL spectra were analyzed using a PicoQuant FluoQuant 300. The *J*–*V* curves of the hybrid PSCs were measured using a Keithley 2400 source under AM1.5G illumination at 100 mW cm^{-2}. EQE spectra of the hybrid PSCs were measured by a Q Test Station 500TI system (Crowntech, Inc. USA). EIS analysis was performed by a Zahner Electrochemical Workstation. Time-resolved fsTA measurements were made utilizing a commercial TA system (Time-Tech Spectra, LLC) equipped with a high-speed spectrometer (Ultrafast systems, HELIOS) and a regeneratively amplified Ti:sapphire laser (Light Conversion, 1030 nm, 150 fs and 100 kHz repetition). The PSCs were encapsulated in a N_2 glove box with cover glasses; encapsulation materials were multicomponent polyurean and UV adhesive. The operational stability of the encapsulated cells was measured at 30 °C under a white light emitting diode lamp with 16-channel thin film photovoltaic maximum power point tracking test system (YH-VMPP-16).

Supporting Information

Supporting Information is available from the Wiley Online Library or from the author.

Acknowledgements

The authors acknowledge support from the National Natural Science Foundation of China (62074095), the National Key Research and Development Program of China (2016YFA0202403), the Fundamental Research Funds for the Central Universities (GK202002001), the 111 Project (GK202002001), and the DNL Cooperation Fund CAS (DNL180311).

Conflict of Interest

The authors declare no conflict of interest.

Data Availability Statement

Research data are not shared.

Keywords

dimer complexes, high efficiency, methyl haloacetate, perovskite solar cells

Received: March 13, 2022
Revised: May 4, 2022
Published online:

[1] W. S. Yang, J. H. Noh, N. J. Jeon, Y. C. Kim, S. Ryu, J. Seo, S. I. Seok, *Science* **2015**, *348*, 1234.
[2] T. H. Wu, Z. Z. Qin, Y. B. Wang, Y. Z. Wu, W. Chen, S. F. Zhang, M. L. Cai, S. Y. Dai, J. Zhang, J. Liu, Z. M. Zhou, X. Liu, H. Segawa, H. R. Tan, Q. W. Tang, J. F. Fang, Y. W. Li, L. M. Ding, Z. J. Ning, Y. B. Qi, Y. Q. Zhang, L. Y. Han, *Nano-Micro Lett.* **2021**, *13*, 152.
[3] A. R. b. M. Yusoff, M. Vasilopoulou, D. G. Georgiadou, L. C. Palilis, A. Abate, M. K. Nazeeruddin, *Energy Environ. Sci.* **2021**, *14*, 2906.
[4] F. Fabregat-Santiago, J. Bisquert, L. Cevey, P. Chen, M. Wang, S. M. Zakeeruddin, M. Grätetzel, *J. Am. Chem. Soc.* **2009**, *131*, 558.
[5] NREL, Best Research-Cell Efficiency Chart, https://www.nrel.gov/pv/cell-efficiency.html (accessed: December 2021).
[6] H. Min, D. Y. Lee, J. Kim, G. Kim, K. S. Lee, J. Kim, M. J. Paik, Y. K. Kim, K. S. Kim, M. G. Kim, T. J. Shin, S. I. Seok, *Nature* **2021**, *598*, 444.
[7] A. Kojima, K. Teshima, Y. Shirai, T. Miyasaka, *J. Am. Chem. Soc.* **2009**, *131*, 6050.
[8] M. C. Qin, J. Cao, T. K. Zhang, J. Q. Mai, T.-K. Lau, S. Zhou, Y. Zhou, J. Y. Wang, Y.-J. Hsu, N. Zhao, J. B. Xu, X. W. Zhan, X. H. Lu, *Adv. Energy Mater.* **2018**, *8*, 1703399.
[9] C. B. Wang, Y. T. Zhang, F. D. Gu, Z. R. Zhao, H. S. Li, H. Jiang, Z. Q. Bian, Z. W. Liu, *Matter* **2021**, *4*, 709.
[10] H. P. Zhou, Q. Chen, G. Li, S. Luo, T.-B. Song, H.-S. Duan, Z. R. Hong, J. B. You, Y. S. Liu, Y. Yang, *Science* **2014**, *345*, 543.
[11] H. Min, M. Kim, S.-U. Lee, H. Kim, G. Kim, K. Choi, J. H. Lee, S. I. Seok, *Science* **2019**, *366*, 749.
[12] C. R. Kagan, D. B. Mitzi, C. D. Dimitrakopoulos, *Science* **1999**, *286*, 945.
[13] Y. J. Fang, Q. F. Dong, Y. C. Shao, Y. B. Yuan, J. S. Huang, *Nat. Photonics* **2015**, *9*, 679.
[14] S. S. Chen, X. Z. Dai, S. Xu, H. Y. Jiao, L. Zhao, J. S. Huang, *Science* **2021**, *373*, 902.
[15] B. Wang, H. Li, Q. Q. Dai, M. Zhang, Z. G. Zou, J.-L. Brédas, Z. Q. Lin, *Angew. Chem., Int. Ed.* **2021**, *60*, 17664.
[16] Q. Cao, J. B. Yang, T. Wang, Y. K. Li, X. Y. Pu, J. S. Zhao, Y. X. Zhang, H. Zhou, X. Q. Li, X. H. Li, *Energy Environ. Sci.* **2021**, *14*, 5406.
[17] Y. Huang, L. Li, Z. H. Liu, H. Y. Jiao, Y. Q. He, X. G. Wang, R. Zhu, D. Wang, J. L. Sun, Q. Chen, H. P. Zhou, *J. Mater. Chem. A* **2017**, *5*, 8537.
[18] W. Li, M. U. Rothmann, Y. Zhu, W. J. Chen, C. Q. Yang, Y. B. Yuan, Y. Y. Choo, X. M. Wen, Y. B. Cheng, U. Bach, J. Etheridge, *Nat. Energy* **2021**, *6*, 624.
[19] J. J. Yoo, G. Seo, M. R. Chua, T. G. Park, Y. L. Lu, F. Rotermund, Y.-K. Kim, C. S. Moon, N. J. Jeon, J.-P. Correa-Baena, V. Bulović, S. S. Shin, M. G. Bawendi1, J. Seo, *Nature* **2021**, *590*, 587.
[20] J. Jeong, M. Kim, J. Seo, H. Z. Lu, P. Ahlawat, A. Mishra, Y. G. Yang, M. A. Hope, F. T. Eickemeyer, M. Kim, Y. J. Yoon, I. W. Choi, B. P. Darwich, S. J. Choi, Y. Jo, J. H. Lee, B. Walker, S. M. Zakeeruddin, L. Emsley, U. Rothlisberger, A. Hagfeldt, D. S. Kim, M. Grätzel, J. Y. Kim, *Nature* **2021**, *592*, 381.
[21] W. Hui, L. F. Chao, H. Lu, F. Xia, Q. Wei, Z. H. Su, T. T. Niu, L. Tao, B. Du, D. L. Li, Y. Wang, H. Dong, S. W. Zuo, B. X. Li, W. Shi, X. Q. Ran, P. Li, H. Zhang, Z. B. Wu, C. X. Ran, L. Song, G. C. Xing, X. Y. Gao, J. Zhang, Y. D. Xia, Y. H. Chen, W. Huang, *Science* **2021**, *371*, 1359.
[22] X. J. Zhu, M. Y. Du, J. S. Feng, H. Wang, Z. Xu, L. K. Wang, S. N. Zuo, C. Y. Wang, Z. Y. Wang, C. Zhang, X. D. Ren, S. Priya, D. Yang, S. Z. Liu, *Angew. Chem., Int. Ed.* **2021**, *60*, 4238.
[23] S. Akin, N. Arora, S. M. Zakeeruddin, M. Grätzel, R. H. Friend, M. I. Dar, *Adv. Energy Mater.* **2020**, *10*, 1903090.
[24] H. Su, J. Zhang, Y. J. Hu, X. Y. Du, Y. Yang, J. X. You, L. L. Gao, S. Z. Liu, *Adv. Energy Mater.* **2021**, *11*, 2101454.
[25] Z. H. Zhang, Y. F. Gao, Z. C. Li, L. Qiao, Q. Xiong, L. H. Deng, Z. L. Zhang, R. Long, Q. Zhou, Y. T. Du, Z. Lan, Y. F. Zhao, C. Li, K. Müllen, P. Gao, *Adv. Mater.* **2021**, *33*, 2008405.
[26] G. Li, T. Y. Zhang, N. J. Guo, F. Xu, X. F. Qian, Y. X. Zhao, *Angew. Chem., Int. Ed.* **2016**, *55*, 13460.
[27] Y. Zhang, G. Grancini, Y. Q. Feng, A. M. Asiri, M. K. Nazeeruddin, *ACS Energy Lett.* **2017**, *2*, 802.
[28] H. W. Zhu, Y. H. Liu, F. T. Eickemeyer, L. F. Pan, D. Ren, M. A. R. Preciado, B. Carlsen, B. W. Yang, X. F. Dong, Z. W. Wang, H. L. Liu, S. R. Wang, S. M. Zakeeruddin, A. Hagfeldt, M. I. Dar, X. G. Li, M. Grätzel, *Adv. Mater.* **2020**, *32*, 1907757.
[29] K. Jung, J. Lee, C. Im, J. Do, J. Kim, W.-S. Chae, M.-J. Lee, *ACS Energy Lett.* **2018**, *3*, 2410.
[30] P. Caprioglio, D. S. Cruz, S. Caicedo-Davila, F. S. Zu, A. A. Sutanto, F. P. Camargo, L. Kegelmann, D. Meggiolaro, L. Gregori, C. M. Wolff, B. Stiller, L. P. Toro, H. Kobler, B. Li, E. G. Partida, I. Lauermann, A. Abate, N. Koch, F. D. Angelis, B. Rech, G. Grancini, D. Abou-Ras, M. K. Nazeeruddin, M. Stolterfoht, S. Albrecht, M. Antonietti, D. Nehe, *Energy Environ. Sci.* **2021**, *14*, 4508.
[31] M. Mateen, Z. Arain, Y. Yang, X. P. Liu, S. Ma, C. Liu, Y. Ding, X. H. Ding, M. L. Cai, S. Y. Dai, *ACS Appl. Mater. Interfaces* **2020**, *12*, 10535.
[32] M.-H. Li, T.-G. Sun, J.-Y. Shao, Y.-D. Wang, J.-S. Hu, Y.-W. Zhong, *Nano Energy* **2021**, *79*, 105462.
[33] T. H. Wu, Y. B. Wang, X. Li, Y. Z. Wu, X. Y. Meng, D. Y. Cui, X. D. Yang, L. Y. Han, *Adv. Energy Mater.* **2019**, *9*, 1803766.
[34] W. Z. Li, J. D. Fan, J. W. Li, G. D. Niu, Y. H. Mai, L. D. Wang, *ACS Appl. Mater. Interfaces* **2016**, *8*, 30107.
[35] H. K. Zhang, M. C. Qin, Z. L. Chen, W. Yu, Z. W. Ren, K. Liu, J. M. Huang, Y. K. Zhang, Q. Liang, H. T. Chandran, P. W. K. Fong, Z. J. Zheng, X. H. Lu, G. Li, *Adv. Mater.* **2021**, *33*, 2100009.
[36] Y. Cai, J. L. Wen, Z. K. Liu, F. Qian, C. Y. Duan, K. He, W. J. Zhao, S. Zhan, S. M. Yang, J. Cui, S. Z. Liu, *J. Energy Chem.* **2022**, *65*, 480.
[37] K. Jung, J.-H. Lee, K. Oh, C. Ima, J. Do, J. Kim, W.-S. Chae, M.-J. Lee, *Nano Energy* **2018**, *54*, 251.
[38] L. Y. Wang, X. Wang, L. Zhu, S.-B. Leng, J. H. Liang, Y. T. Zheng, Z. F. Zhang, Z. A. Zhang, X. X. Liu, F. Liu, C.-C. Chen, *Chem. Eng. J.* **2022**, *430*, 132730.

[39] R. Xia, X.-X. Gao, Y. Zhang, N. Drigo, V. I. E. Queloz, F. F. Tirani, R. Scopelliti, Z. J. Huang, X. D. Fang, S. Kinge, Z. F. Fei, C. Roldán-Carmona, M. K. Nazeeruddin, P. J. Dyson, *Adv. Mater.* **2020**, *32*, 2003801.
[40] B. J. Kim, G. Boschloo, *Nanoscale* **2021**, *13*, 11478.
[41] F. Qian, S. H. Yuan, Y. Cai, Y. Han, H. Zhao, J. Sun, Z. K. Liu, S. Z. Liu, *Sol. RRL* **2019**, *3*, 1900072.
[42] W. J. Zhao, J. Xu, K. He, Y. Cai, Y. Han, S. M. Yang, S. Zhan, D. P. Wang, Z. K. Liu, S. Z. Liu, *Nano-Micro Lett.* **2021**, *13*, 169.
[43] Y. H. Chen, X. Q. Yang, P. Y. Liu, W. Wang, R. Ran, W. Zhou, Z. P. Shao, *Sol. RRL* **2021**, *5*, 2000621.
[44] S. H. Yuan, Y. Cai, S. M. Yang, H. Zhao, F. Qian, Y. Han, J. Sun, Z. K. Liu, S. Z. Liu, *Sol. RRL* **2019**, *3*, 1900220.
[45] N. K. Noel, M. Congiu, A. J. Ramadan, S. Fearn, D. P. McMeekin, J. B. Patel, M. B. Johnston, B. Wenger, H. J. Snaith, *Joule* **2017**, *1*, 328.
[46] N. Ali, X. Y. Wang, S. Rauf, S. Attique, A. Khesro, S. Ali, N. Mushta, H. B. Xiao, C. P. PingYang, H. Z. Wu, *Sol. Energy* **2019**, *189*, 325.
[47] S.-P. Cho, S.-N. Kwon, M.-J. Choi, Y.-H. Seo, S.-S. Kim, S.-I. Na, *ACS Appl. Mater. Interfaces* **2020**, *12*, 46846.
[48] L. Zhang, Y. X. Chen, *Appl. Surf. Sci.* **2020**, *502*, 144274.
[49] A. Maqsood, Y. Y. Li, J. Meng, D. D. Song, B. Qiao, S. L. Zhao, Z. Xu, *Nanoscale Res. Lett.* **2020**, *15*, 89.
[50] Q. S. Dong, M. Chen, Y. H. Liu, F. T. Eickemeyer, W. D. Zhao, Z. H. Dai, Y. F. Yin, C. Jiang, J. S. Feng, S. Y. Jin, S. Z. Liu, S. M. Zakeeruddin, M. Grätzel, N. P. Padture, Y. T. Shi, *Joule* **2021**, *5*, 1587.
[51] M. Park, J.-Y. Kim, H. J. Son, C.-H. Lee, S. S. Jang, M. J. Ko, *Nano Energy* **2016**, *26*, 208.
[52] Q. S. Dong, C. Zhu, M. Chen, C. Jiang, J. Y. Guo, Y. L. Feng, Z. H. Dai, S. K. Yadavalli, M. Y. Hu, X. Cao, Y. Q. Li, Y. Z. Huang, Z. Liu, Y. T. Shi1, L. D. Wang, N. P. Padture, Y. Y. Zhou, *Nat. Commun.* **2021**, *12*, 973.
[53] G. H. Wu, H. Li, J. Cui, Y. H. Zhang, S. Olthof, S. Chen, Z. K. Liu, D. P. Wang, S. Z. Liu, *Adv. Sci.* **2020**, *7*, 1903250.
[54] X. Guo, B. Zhao, K. X. Xu, S. M. Yang, Z. K. Liu, Y. Han, J. Xu, D. F. Xu, Z. A. Tan, S. Z. Liu, *Small* **2021**, *17*, 2102272.
[55] S. M. Yang, W. D. Liu, Y. Han, Z. K. Liu, W. J. Zhao, C. Y. Duan, Y. H. Che, H. S. Gu, Y. B. Li, S. Z. Liu, *Adv. Energy Mater.* **2020**, *10*, 2002882.
[56] P. J. Chao, L. Z. Liu, J. D. Zhou, J. F. Qu, D. Z. Mo, H. Meng, Z. Q. Xie, F. He, Y. G. Ma, *ACS Appl. Energy Mater.* **2018**, *1*, 6549.
[57] J. Qing, X.-K. Liu, M. J. Li, F. Liu, Z. C. Yuan, E. Tiukalova, Z. B. Yan, M. Duchamp, S. Chen, Y. M. Wang, S. Bai, J.-M. Liu, H. J. Snaith, C.-S. Lee, T. C. Sum, F. Gao, *Adv. Energy Mater.* **2018**, *8*, 1800185.
[58] Y. Han, H. Zhao, C. Y. Duan, S. M. Yang, Z. Yang, Z. K. Liu, S. Z. Liu, *Adv. Funct. Mater.* **2020**, *30*, 1909972.
[59] H. Zhao, Y. Han, Z. Xu, C. Y. Duan, S. M. Yang, S. H. Yuan, Z. Yang, Z. K. Liu, S. Z. Liu, *Adv. Energy Mater.* **2019**, *9*, 1902279.
[60] C. Y. Duan, J. Cui, M. M. Zhang, Y. Han, S. M. Yang, H. Zhao, H. T. Bian, J. X. Yao, K. Zhao, Z. K. Liu, S. Z. Liu, *Adv. Energy Mater.* **2020**, *10*, 2000691.
[61] X. J. Gu, W. C. Xiang, Q. W. Tian, S. Z. Liu, *Angew. Chem., Int. Ed.* **2021**, *60*, 23164.
[62] S. M. Yang, J. L. Wen, Z. K. Liu, Y. H. Che, J. Xu, J. G. Wang, D. F. Xu, N. Y. Yuan, J. N. Ding, Y. W. Duan, S. Z. Liu, *Adv. Energy Mater.* **2021**, *12*, 2103019.